# Supporting Information

# Dual-Responsive and NIR-Driven Free Radical Nanoamplifier with Glutathione Depletion for Enhanced Tumor-Specific Photothermal/Thermodynamic/Chemodynamic Synergistic Therapy

*Fanghui Chen,[a] Xichen Zhang,[a] Zining Wang,[a] Chensen Xu,[a] Jinzhong Hu,[a] Ling Liu,*[,c] Jiancheng Zhou,*[,a] Baiwang Sun,*[,a,b]*

[a] School of Chemistry and Chemical Engineering, Southeast University, Nanjing 211189, China

[b] Jiangsu Province Hi-Tech Key Laboratory for Biomedical Research, Southeast University, Nanjing 211189, China

[c] Department of Infectious Diseases, Hospital of Integrated Traditional Chinese and Western Medicine Affiliated with Nanjing University of Chinese Medicine, Nanjing 210028, China

* Corresponding authors, E-mail addresses: lingliumed@163.com (Ling Liu); jczhou@seu.edu.cn (Jiancheng Zhou); chmsunbw@seu.edu.cn (Baiwang Sun)

# Supplementary Methods

**Materials.** 1,3,5-trimethylbenzene (TMB), dopamine hydrochloride, ammonia hydroxide ($NH_4OH$, 28-30 wt%), Tris-HCl buffer (pH 8.5), methylene blue (MB), glutathione (GSH), 2,2'-azobis[2-(2-imidazolin-2-yl) propane] dihydrochloride (AIPH), hydrogen peroxide ($H_2O_2$, 30 wt%), and fluorescein isothiocyanate (FITC) were purchased from Aladdin Biochemical Technology Co. Ltd. (Shanghai, China). Pluronic F127, copper (II) chloride ($CuCl_2$), tannic acid (TA), hyaluronate (HA), 5,5'-dithiobis (2-nitrobenzoic acid) (DTNB), indocyanine green (ICG), and 2,2'-azino-bis(3-ethylbenzothiazoline-6-sulfonicacid) (ABTS) were acquired from Sigma-Aldrich Trading Co. Ltd. (Shanghai, China). RPMI-1640 medium, DMEM medium, fetal bovine serum (FBS), phosphate-buffered saline (PBS), calcein-AM/propidium iodide (PI) stain kit, 2',7'-dichlorodihydrofluorescein diacetate (DCFH-DA), Annexin V-FITC/PI apoptosis detection kit, 4',6-Diamidino-2-phenylindole (DAPI), Lyso-Tracker Red, GSH assay kit, and 3-(4,5-Dimethylthiazol-2-yl)-2,5-diphenyltetrazolium bromide (MTT) were obtained from Jiangsu KeyGen Biotech. Co. Ltd. (Nanjing, China).

**Calculation of the Photothermal Conversion Efficiency.** In order to evaluate the photothermal conversion efficiency (η), the MACTH dispersion (100 μg $mL^{-1}$, 1.0 mL) was irradiated with 808 nm laser (1.0 W $cm^{-2}$) for 600 s, followed by switching off the laser and naturally cooling to ambient temperature. The photothermal conversion efficiency was calculated by the following equation:

$$\eta = \frac{hS(T_{max} - T_{sur}) - Q_{dis}}{I(1 - 10^{-A_{808}})}$$

Where $h$ is the heat transfer coefficient, $S$ is the surface area of the container, $T_{max}$ is the maximum equilibrium temperature of the sample solution, $T_{sur}$ is the surrounding temperature, $Q_{dis}$ is the heat generated by the container and solution under laser irradiation, $I$ is the laser power, and $A_{808}$ is the absorbance of the sample solution at 808 nm.

**Cell Culture.** Human breast adenocarcinoma cell line (MDA-MB-231) and human normal liver cell line (LO2) were obtained from the Cell Bank of the Chinese Academy of Science (Shanghai, China). The MDA-MB-231 and LO2 cells were cultured in DMEM and RPMI-1640 medium respectively, containing 10% FBS and 1% penicillin/streptomycin at 37 °C under 5% of $CO_2$.

## Supplementary Figures

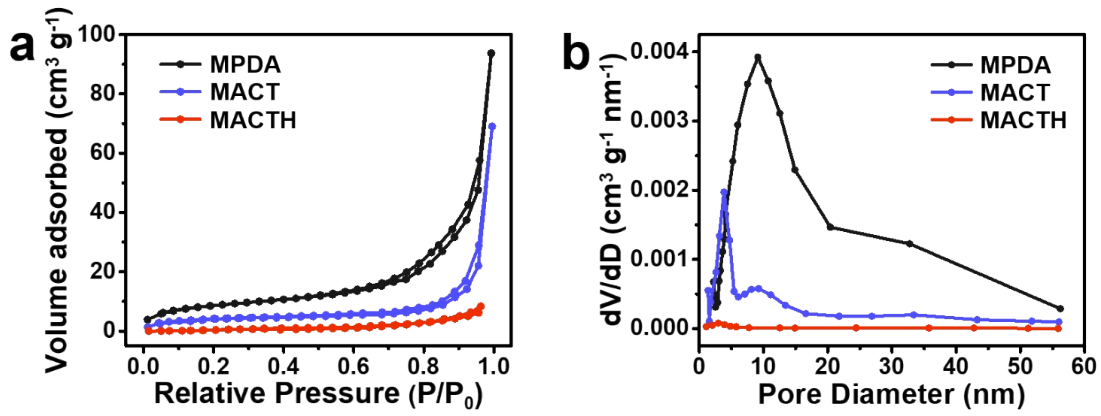


**Fig. S1.** (a) $N_2$ absorption-desorption isotherms and (b) corresponding pore size distribution of MPDA, MACT and MACTH.

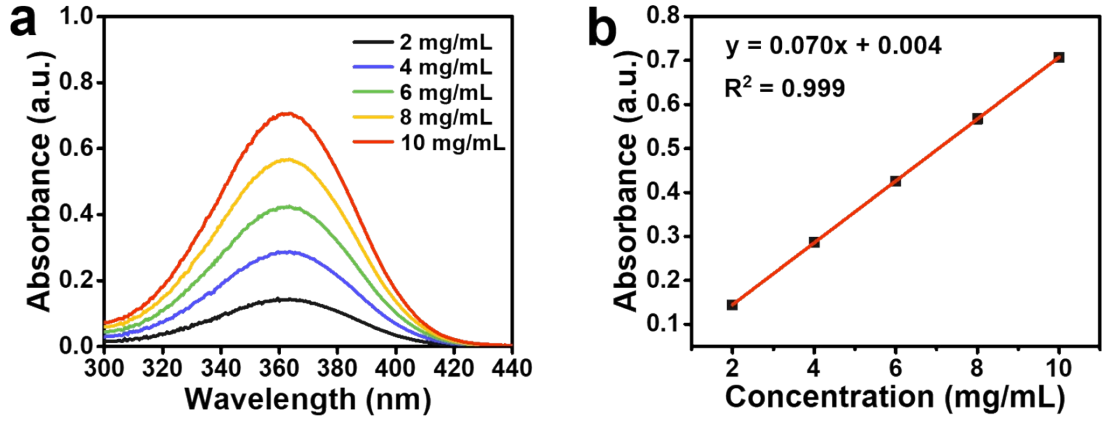


**Fig. S2.** (a) UV-vis absorption spectra of AIPH at different concentrations. (b) Standard curve of AIPH (absorbance *vs.* concentration).

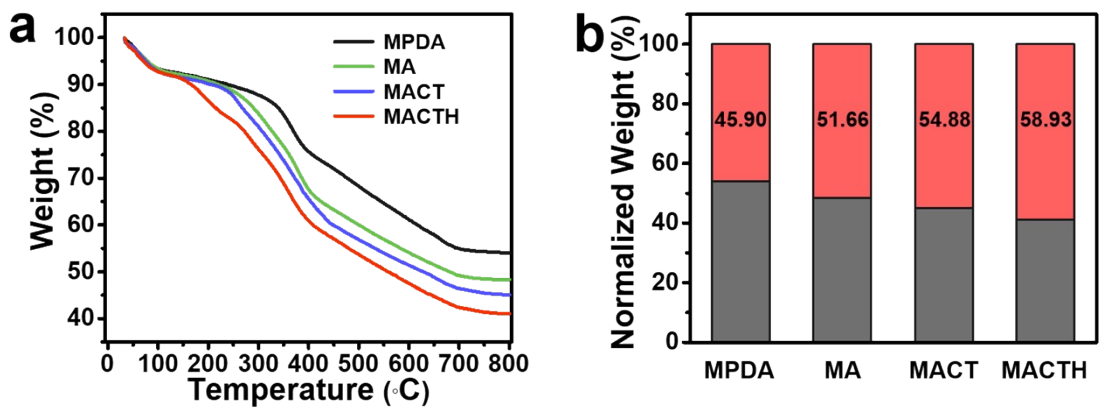


**Fig. S3.** (a) TGA curves and (b) normalized weight loss diagram of MPDA, MA, MACT and MACTH.

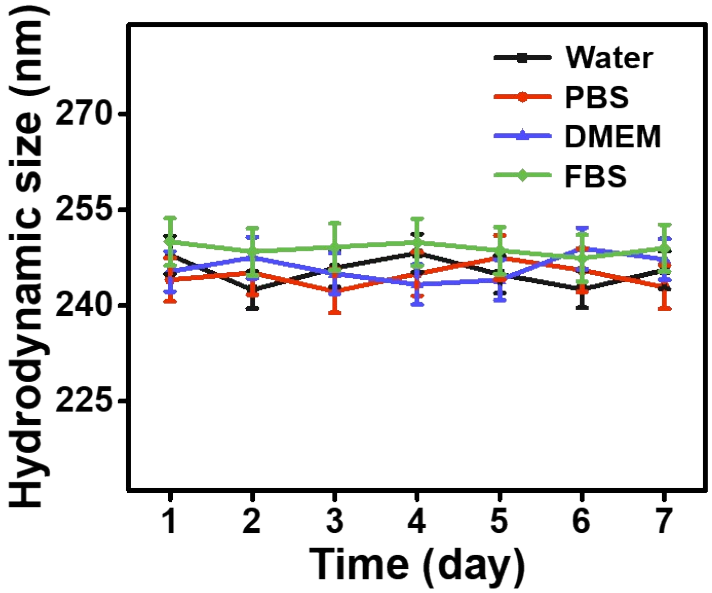


**Fig. S4.** The hydrodynamic size changes of MACTH in various physiological media, including water, PBS, DMEM and FBS for 7 days.

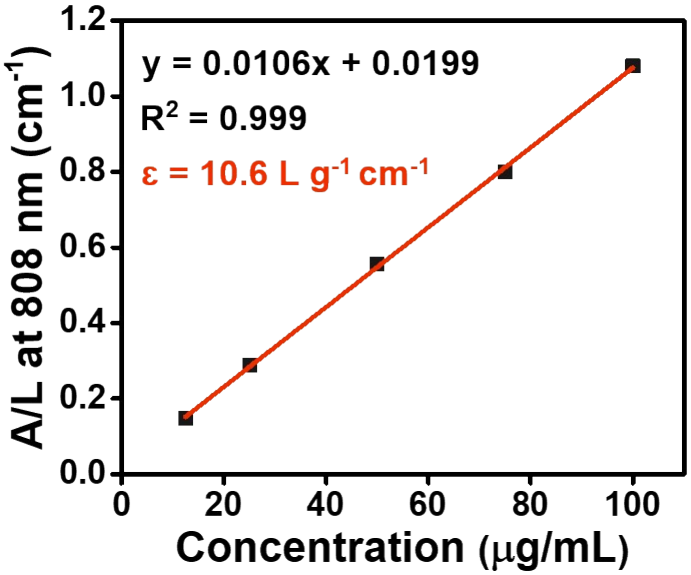


**Fig. S5.** Normalized absorbance of MACTH aqueous solution at 808 nm with different concentrations.

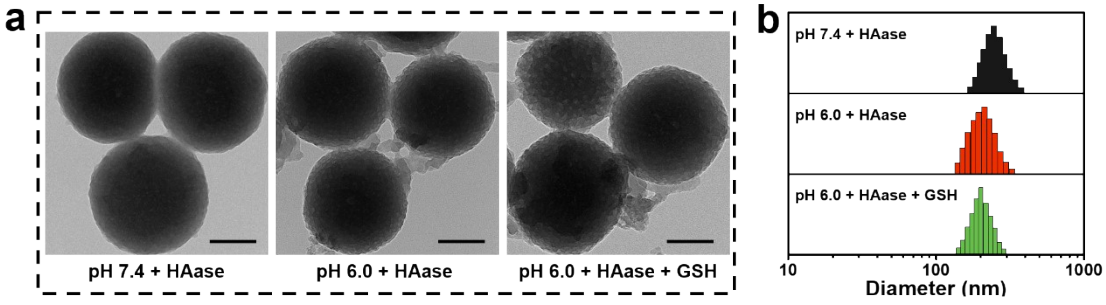


**Fig. S6.** (a) TEM images and (b) hydrodynamic size distributions of MACTH after various treatments for 24 h (scale bars: 100 nm).

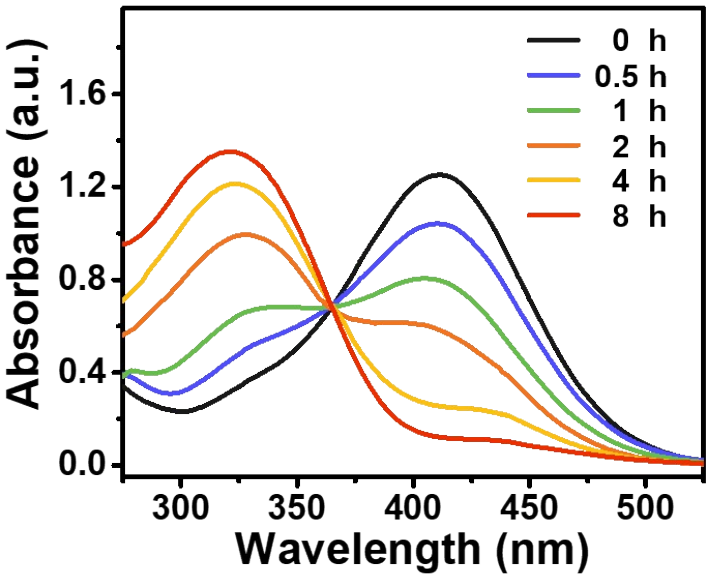


**Fig. S7.** GSH depletion by MACT (50 μg $mL^{-1}$) at different time points.

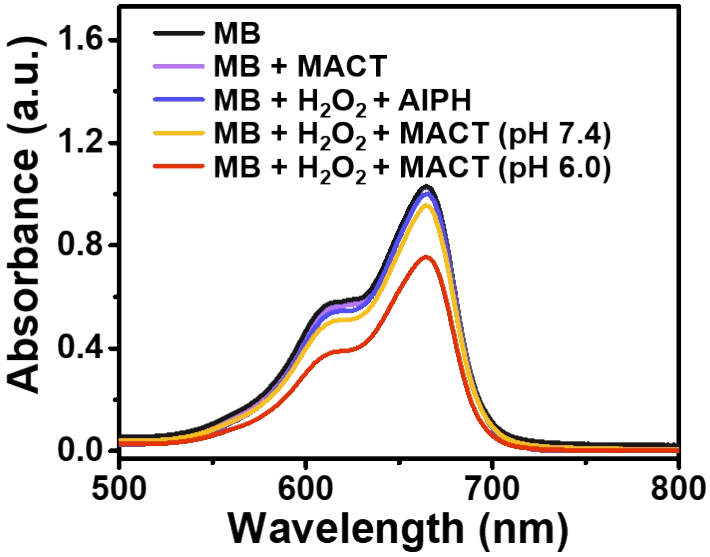


**Fig. S8.** UV-vis absorption spectra of MB after treatment with different samples (AIPH: 20.3 μg $mL^{-1}$, MACT: 200 μg $mL^{-1}$, $H_2O_2$: 8 mM).

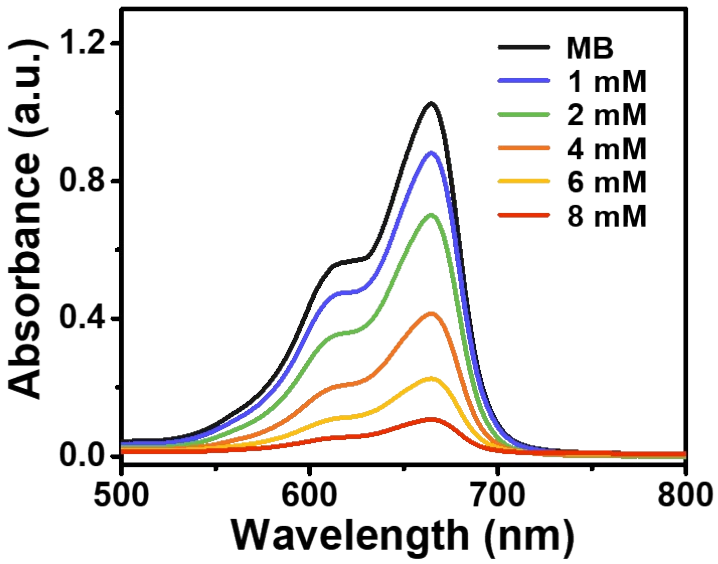


**Fig. S9.** MB degradation by GSH-treated MACT plus different concentrations of $H_2O_2$ at pH 6.0 (MACT: 200 μg $mL^{-1}$, GSH: 2 mM).

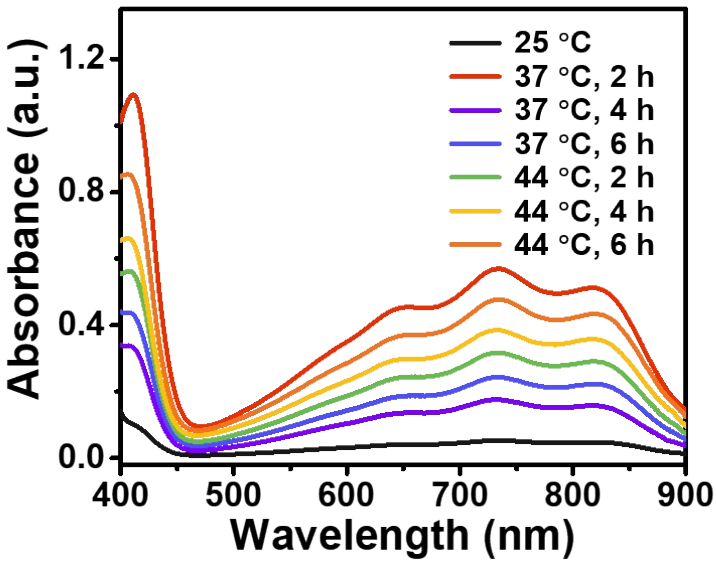


**Fig. S10.** Generation of $ABTS^{+\cdot}$ as induced by the free radicals produced from AIPH at different temperatures and time points.

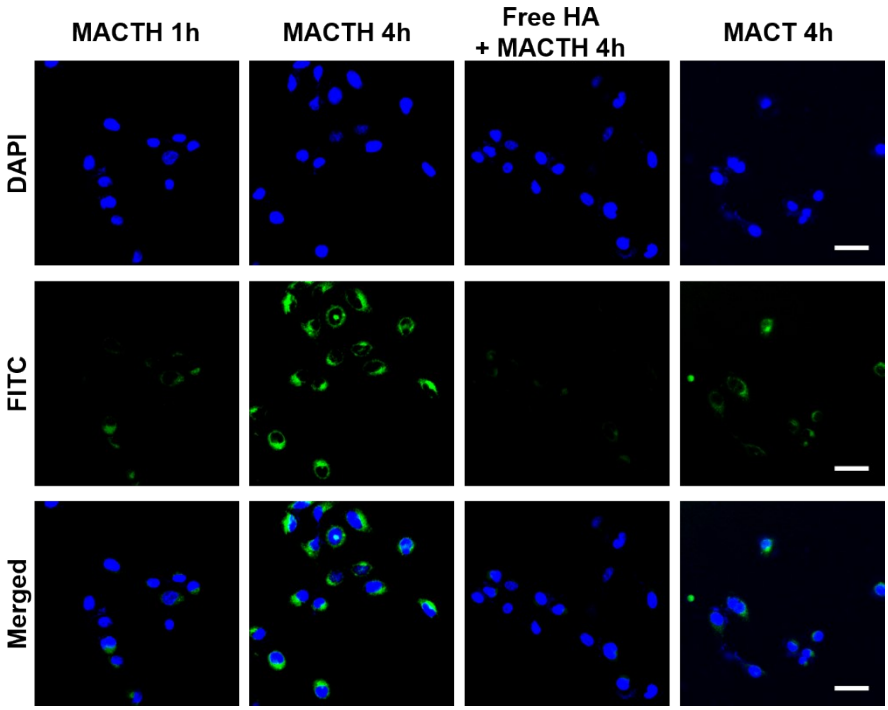


**Fig. S11.** CLSM images of MDA-MB-231 cells treated with FITC-labeled MACT and MACTH (scale bars: 50 μm).

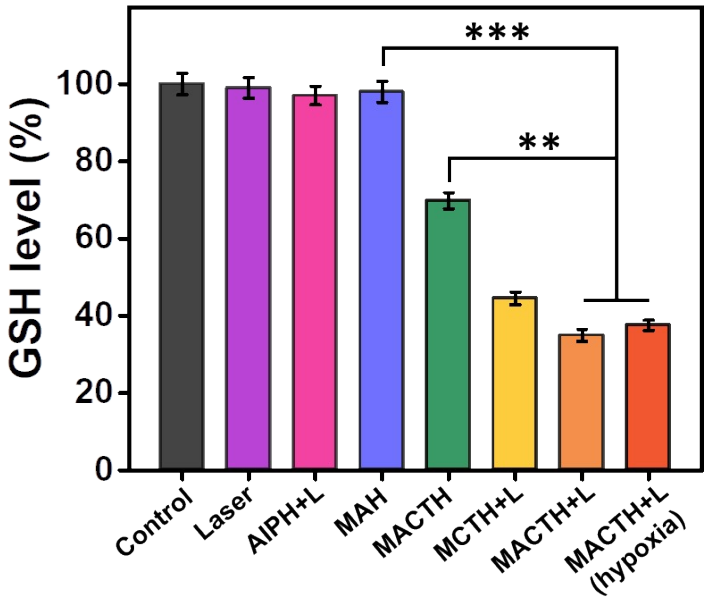


**Fig. S12.** GSH level in MDA-MB-231 cells after different treatments.

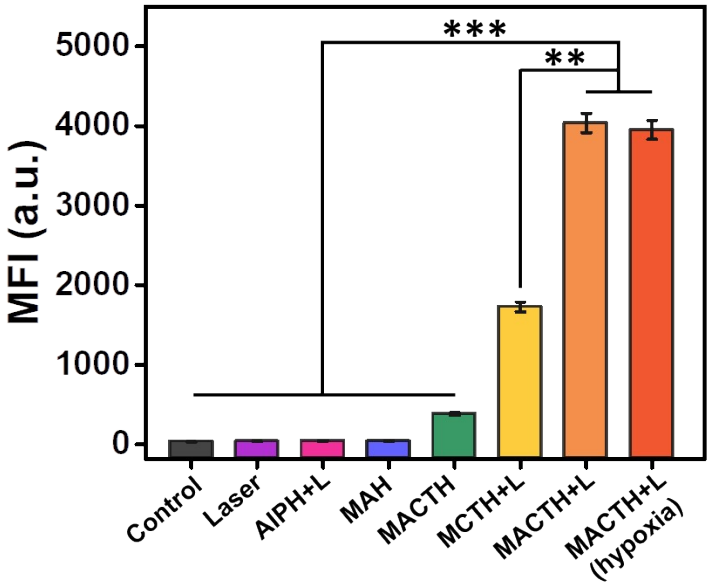


**Fig. S13.** The quantitative mean fluorescence intensity (MFI) of intracellular DCF corresponding to Fig. 4c.

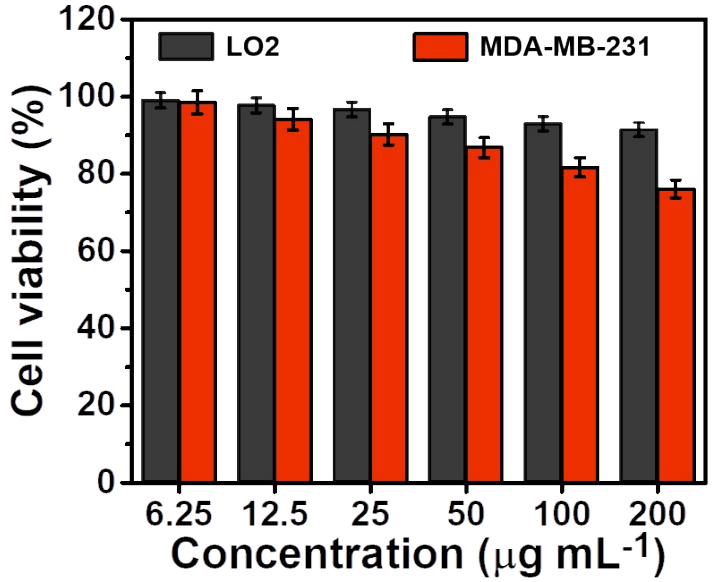


**Fig. S14.** Cell viability of LO2 and MDA-MB-231 cells after treatment with gradient concentrations of MACTH for 24 h.

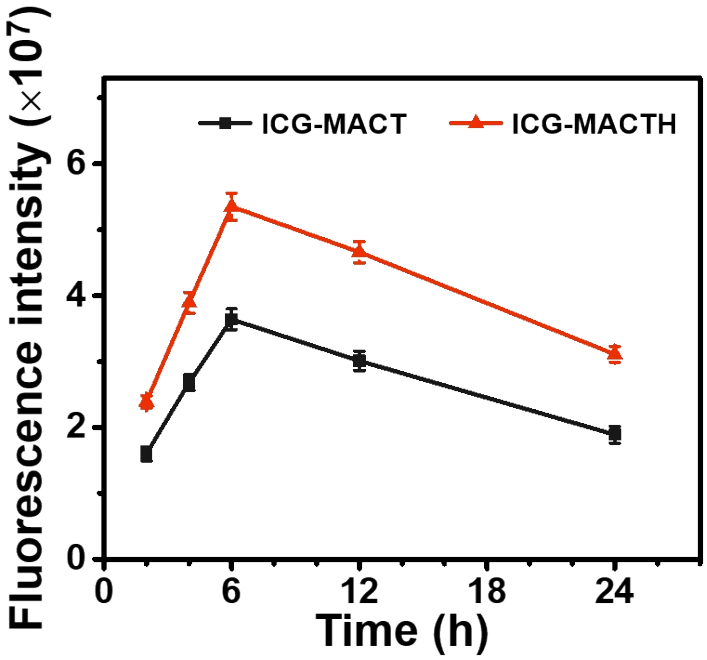


**Fig. S15.** Fluorescence intensity of the tumor sites at different time points corresponding to Fig. 5b.

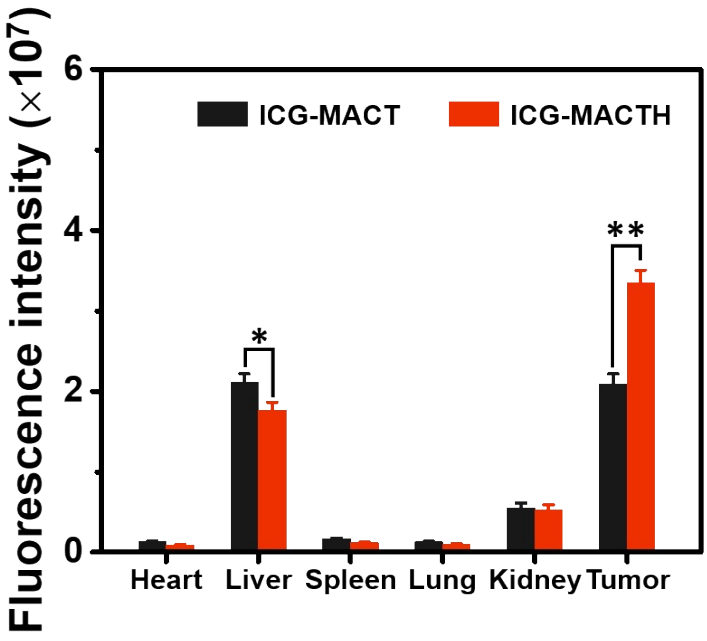


**Fig. S16.** Fluorescence intensity of major organs and tumor corresponding to Fig. 5c.

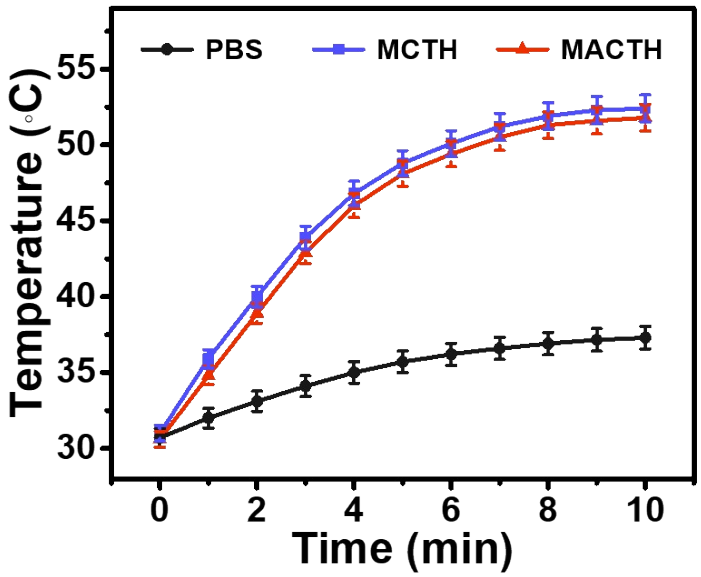


**Fig. S17.** Temperature elevation curves of tumor regions after various treatments corresponding to Fig. 5d.

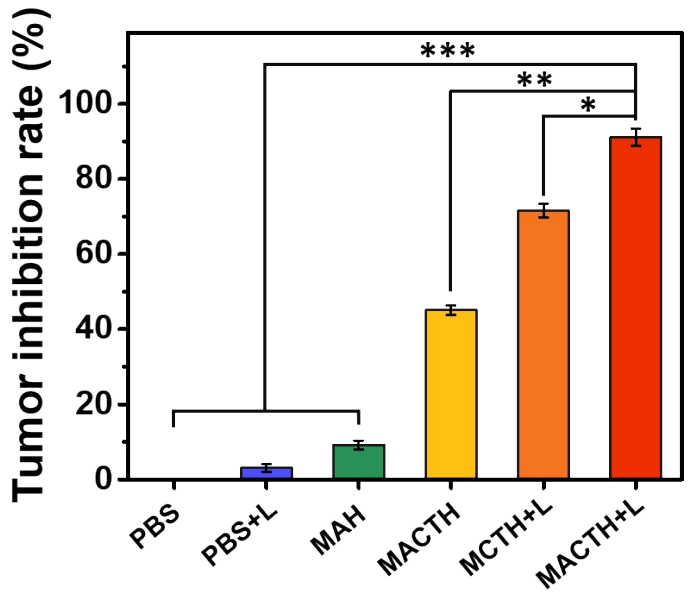


**Fig. S18.** Tumor inhibition rate of MDA-MB-231 tumor-bearing nude mice with various treatments.

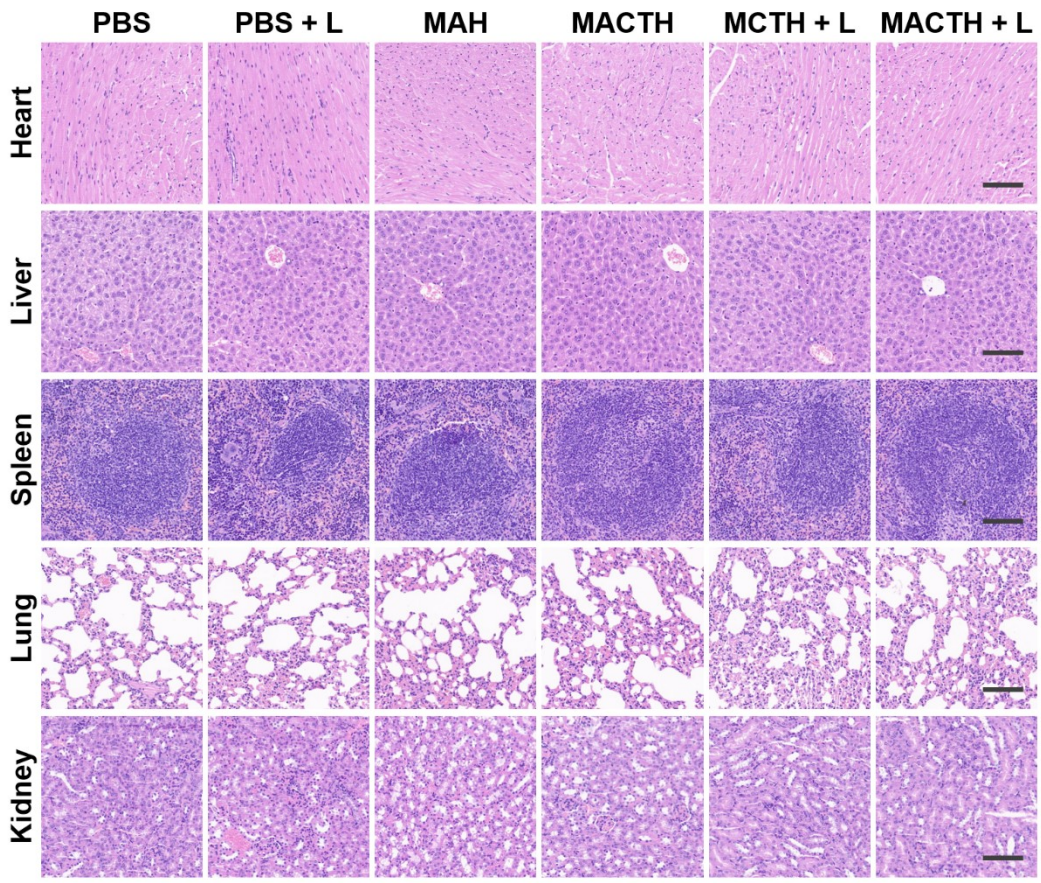


**Fig. S19.** Histopathological examination of the main organs after different treatments (scale bar: 100 μm).